A remarkable solar-blind ultraviolet nonlinear optical crystal with comprehensive performance and enhanced thermal stability

Jialin Zeng[a,b], Shuangcheng Li[a], Ruibiao Fu[*a,d], Zilong Geng[a,d], Yiting Luo[a,b], Senfu Lei[a], Zuju Ma[*c],

[a]State Key Laboratory of Structural Chemistry, Fujian Institute of Research on the Structure of Matter, Chinese Academy of Sciences, Fuzhou, Fujian 350002, P. R. China

[b]College of Chemistry and Materials Science, Fujian Normal University, Fuzhou, Fujian 350007, P. R. China

[c]School of Environmental and Materials Engineering, Yantai University, Yantai, 264005, P. R. China

[d]University of Chinese Academy of Sciences, Beijing 100049, China

[*]Corresponding author. *E-mail:* furb@fjirsm.ac.cn (R. B. Fu); zjma@outlook.com (Z. J. Ma).

.

Experimental Section

1. Reagents

Iminodiacetic acid ($HN(CH_2COOH)_2$, 98%), potassium carbonate (K_2CO_3, 99%) and sodium carbonate (Na_2CO_3, 99.8%) were purchased from commercial sources and used as received without further purification.

2. Synthesis

Crystals of $K[H_2N(CH_2COO)_2]$ were synthesized by a feasible volatilization method. The crystal of $K[H_2N(CH_2COO)_2]$ can grow up to a large size of 15 × 9 × 5 mm^3 (Figure S1). The reaction mixtures of $HN(CH_2COOH)_2$ (2.662 g, 0.02 mol) and K_2CO_3 (1.3821 g, 0.01 mol) were dissolved in 5 mL distilled water and then evaporated at room temperature for 3 days. Colorless crystals of $K[H_2N(CH_2COO)_2]$ were obtained. The yield is about 50% based on iminodiacetic acid. Experimental PXRD patterns match well with those simulated from single-crystal X-ray diffraction data that confirms its phase purity (Figure S2). Energy dispersive X-ray spectroscopy (EDS) spectrum identifies the coexistences of K, C, N and O elements (Figure S4). In IR spectrum of $K[H_2N(CH_2COO)_2]$, two strong absorption bands at 1614 and 1375 cm^{-1} are attributed to the stretching vibration of the carboxylate group (Figure S5). And the weak peak at 3015 cm^{-1} belongs to the N-H strethching vibration. Meanwhile, the absorption peak at 1284 cm^{-1} can be assigned to the stretching vibration of the C-N bond. Thus, its IR spectrum supports the presence of the iminodiacetate group. Anal. Calcd. for $K[H_2N(CH_2COO)_2]$: C 28.06 %, N 8.18 %, H 3.53 %. Found: C 27.77 %, N 7.88 %, H 3.57 %. Thus, elemental analysis of C, H and N for $K[H_2N(CH_2COO)_2]$ are in good agreement with respective theoretical values.

Colorless crystals of $[Na_3(H_2O)_2][H_2N(CH_2COO)_2]_3 \cdot H_2O$ were obtained with the same volatilization method by the replacement of K_2CO_3 with Na_2CO_3. The yield is approximately 70% based on iminodiacetic acid. Its phase purity is validated by the fact that experimental PXRD patterns are in good agreement with those simulated from single-crystal X-ray diffraction data (Figure S3). In the IR spectrum of $[Na_3(H_2O)_2][H_2N(CH_2COO)_2]_3 \cdot H_2O$ (Figure S6), there are two strong absorption

bands centered at 1614 and 1379 cm^{-1} are attributed to the stretching vibration of the carboxylate group. A faint peak at 2991 cm^{-1} pertains to the stretching vibration of the N-H. At the same time, a absorption peak at 3306 cm^{-1} belongs to the stretching vibration of the O-H of water molecules. Anal. Calcd. for $[Na_3(H_2O)_2][H_2N(CH_2COO)_2]_3 \cdot H_2O$: C 27.75 %, N 8.09 %, H 4.66 %. Found: C 28.05 %, N 8.20 %, H 4.94 %. Thereby, elemental analysis of C, H and N for $[Na_3(H_2O)_2][H_2N(CH_2COO)_2]_3 \cdot H_2O$ accord well with respective theoretical values.

3. Single-crystal X-ray diffraction

Single-crystal X-ray diffraction data for a colorless transparent crystal of $K[H_2N(CH_2COO)_2]$ were collected on a Rigaku XtaLAB Synergy-R diffractometer equipped with a graphite-monochromated Mo Kα radiation (λ(Mo-Kα) = 0.71073 Å). Data reduction was integrated by using the CrysAlisPro 1.171.43.101 program. While single-crystal X-ray diffraction data for $[Na_3(H_2O)_2][H_2N(CH_2COO)_2]_3 \cdot H_2O$ were collected on a Rigaku XtaLAB Synergy diffractometer equipped with a graphite-monochromated Cu Kα radiation (λ(Cu-Kα) = 1.54184 Å). The CrysAlisPro 1.171.41.98a program was performed to integrate data reduction. The direct method with the aid of the SHELXT has been carried out to solve their structures, and further refined by the SHELXL full-matrix least-squares program.[1,2] Furthermore, we have checked for possible higher symmetry with the aid of the PLATON.[3] However, no higher symmetries are suggested. Tables S1-S2 list their crystallographic data. Atomic coordinates, equivalent isotropic displacement parameters and bond valence sum (BVS), anisotropic displacement parameters, as well as selected bond lengths and angles are summarized in Tables S3-8. CCDC 2393545 for $K[H_2N(CH_2COO)_2]$ and 2393546 for $[Na_3(H_2O)_2][H_2N(CH_2COO)_2]_3 \cdot H_2O$.

4. Powder X-ray Diffraction

PXRD measurement was carried out at room temperature on a Rigaku Miniflex 600 diffractometer with a Cu Kα radiation (λ = 1.540598 Å). All data were obtained in the 2θ range of 5-55^o with a step size of 0.02^o.

5. Thermogravimetric and Differential Thermal Analysis (TGA-DTA)

TGA-DTA were employed on a NETZCH STA 449F3 thermal analysis instrument by

using an Al_2O_3 crucible as a reference. In a flowing nitrogen gas, the temperature was raised from 30 to 800 ^oC at a heating rate of 10 $^oC \cdot min^{-1}$.

6. EDS and elemental analyses

Microprobe elemental analyses were performed by using a field emission scanning electron microscope (FESEM, JSM6700F) with an EDS (Oxford INCA). C, N and H analyses were carried out with a Vario EL III element analyzer.

7. Optical spectroscopy

IR spectrum was recorded on a VERTEX70 FT-IR spectrometer instrument at room temperature according to attenuated total reflectance method. The crystal sample was tightly fitted to the total reflection crystal and then the data were collected within the wavelength range of 400~4000 cm^{-1}. What's more, UV-Vis-NIR diffuse reflectance spectrum spanning over 190 to 2500 nm was performed on a PerkinElmer Lambda 950 ultraviolet/visible/near-infrared spectrophotometer with $BaSO_4$ as the standard reference. The reflection spectrum was converted into the absorption spectrum based on the Kubelka-Munk function: $\alpha/S = F(R) = (1-R)^2/2R$, (where S is the scattering coefficient, α is the absorption coefficient, and R is the reflectance).[4,5]

8. SHG and laser damage threshold (LDT) measurements

Powder SHG response was measured on a pulsed Q-switched Nd: YAG solid-state laser by a modified Kurtz-Perry method with the wavelength of 1064 nm and 532 nm under room temperature.[6] Crystalline samples, microcrystallines KDP and BBO as the references were ground and sieved into progressively increasing particle size ranges: 25-53, 53-75, 75-109, 109-150, 150-212 and 212-355 μm. LDT of $K[H_2N(CH_2COO)_2]$ was tested on as-synthesized crystals under a 1064 nm laser source (10 ns, 1 Hz and 0.2 cm^2 for laser spot area) within the particle-size range of 0.5-1.0 mm. The energy of the laser emission was gradually enhanced until the color of the sample changed.

9. Computational details

In order to study the origin of NLO performance, single-crystal data of $K[H_2N(CH_2COO)_2]$ was applied for theoretical calculations. Our density functional theory (DFT) calculations have been carried out by using the Vienna *ab initio* simulation package (VASP)[7,8] with the Perdew-Burke-Ernzerhof (PBE)[9] exchange

correlation functional. The projected augmented wave (PAW)[10] potentials have been used to treat the ion-electron interactions. A Γ-centered 9 × 9 × 9 Monkhorst-Pack grid for the Clillouin zone sampling[11] and a cutoff energy of 500 eV for the plane wave expansion were found to get convergent lattice parameters and self-consistent energies. In calculation of the static $\chi^{(2)}$ coefficients, we adopt the length-gauge formalism derived by Aversa and Sipe[12] and modified by Rashkeevet al[13], which has been proved to be successful in calculating the second order susceptibility for semiconductors and insulators.[14-16] The dynamic SHG coefficient is calculated based on the formula developed by Aversa, Sipe and Rashkeev et al.[12,13]

In the static case, the imaginary part of the static second-order optical susceptibility can be expressed as:

$$\chi^{abc} = \frac{e^3}{\hbar^2\Omega}\sum_{nml,k}\frac{r^{a}_{nm}(r^{b}_{ml}r^{c}_{ln}+r^{c}_{ml}r^{b}_{ln})}{2\omega_{nm}\omega_{ml}\omega_{ln}}[\omega_n f_{ml}+\omega_m f_{ln}+\omega_l f_{nm}]$$

$$+\frac{ie^3}{4\hbar^2\Omega}\sum_{nm,k}\frac{f_{nm}}{\omega^2_{mn}}[r^{a}_{nm}(r^{b}_{mn;c}+r^{c}_{mn;b})+r^{b}_{nm}(r^{a}_{mn;c}+r^{c}_{mn;a})+r^{c}_{nm}(r^{a}_{mn;b}+r^{b}_{mn;a})]$$

where r is the position operator, $\hbar\omega_{nm} = \hbar\omega_n - \hbar\omega_m$ is the energy difference for the bands m and n, $f_{mn} = f_m - f_n$ is the difference of the Fermi distribution functions, subscripts a, b, and c are Cartesian indices, and $r^{b}_{mn;a}$ is the so-called generalized derivative of the coordinate operator in k space.

$$r^{b}_{nm;a} = \frac{r^{a}_{nm}\Delta^{b}_{mn}+r^{b}_{nm}\Delta^{a}_{mn}}{\omega_{nm}}+\frac{i}{\omega_{nm}}\times\sum_{l}(\omega_{lm}r^{a}_{nl}r^{b}_{lm}-\omega_{nl}r^{b}_{nl}r^{a}_{lm})$$

where $\Delta^{a}_{nm} = (p^{a}_{nn} - p^{a}_{mm}) / m$ is the difference between the electronic velocities at the bands n and m.

The $\chi^{(2)}$ coefficients here were calculated from PBE wave functions with a 9 × 9 × 9 k-point grid and about 240 bands (3:1 ratio of conduction to valence bands). A scissor operator has been added to correct the conduction band energy (corrected to the experimental gap), which has been proved to be reliable in predicting the second-order susceptibility for semiconductors and insulators.[17-19]

For an external radiation electric field E, the dipole moment μ_i of a group can be expressed as a Taylor series expansion [14,16]

$$\mu_i = \mu_i^0 + \alpha_{ij}E_j + \frac{1}{2!}\beta_{ijk}E_jE_k + \frac{1}{3!}\gamma_{ijkl}E_jE_kE_l$$

where i, j, k, and l subscripts represent the different Cartesian coordinate components x, y, or z. μ_i^0 is the permanent dipole moment of a group, namely the dipole moment without an applied electric field. Physical quantities α, β and γ correspond to the linear polarizability (α, which corresponds to the linear optical coefficient of a group), first-order hyperpolarizability tensor (β, which is the second-order nonlinear optical coefficient of a group), and second-order hyperpolarizability tensor (γ, which is the third-order nonlinear optical coefficient of a group).

We calculate the static linear polarizability (α) and static first-order hyperpolarizability (β) of [$H_2N(CH_2COO)_2$] groups at the PBE1PBE level [9] of theory with a reasonably large basis set def2TZVP [20,21] by using the Gaussian 09 program.[22] The polarizability anisotropy ($\Delta\alpha$) was obtained by the following formula to reflect the sources of birefringence.[23]

$$\Delta\alpha = \sqrt{\left[\left(\alpha_{xx} - \alpha_{yy}\right)^2 + \left(\alpha_{xx} - \alpha_{zz}\right)^2 + \left(\alpha_{yy} - \alpha_{zz}\right)^2\right]/2}$$

Tables and Figures

Table S1. Crystal data and structure refinements for **$K[H_2N(CH_2COO)_2]$**..

Empirical formula	**$K[H_2N(CH_2COO)_2]$**
Formula weight	171.20
Temperature (K)	287.15
Crystal color	Colorless
Crystal dimensions	$0.5 \times 0.5 \times 0.5$ mm^3
Wavelength (Å)	0.71073
Crystal system	Monoclinic
Space group	$P2_1$
a / Å	5.6639(3)
b / Å	7.1900(5)
c / Å	8.6120(6)
α / °	90
β / °	98.664(6)
γ / °	90
Volume / Å^3	346.71(4)
Z	2
ρ_{calcd} / g·cm^{-3}	1.640
μ / mm^{-1}	0.721
F(000)	176.0
Scan mode	ω scan
Data / restraints / parameters	1703/1/91
2-Theta range for data collection	4.784 to 61.4
Limiting indices	$-7 \leq h \leq 7$, $-10 \leq k \leq 9$, $-12 \leq l \leq 11$
Reflections collected	4694
Independent reflections	1703 [R_{int}=0.0337, R_{sigma}=0.0417]
Completeness	100%
Goodness-of-fit on F^2	1.063
R_1,wR_2 ($I > 2\sigma$) [a]	R_1 = 0.0444, wR_2 = 0.1196
R_1,wR_2 (all data)	R_1 = 0.0496, wR_2 = 0.1233
Largest diff. peak and hole/ e·Å^{-3}	0.70 and -0.29
Flack parameter	-0.07(4)
CCDC number	2393545

[a] $R_1 = \Sigma||F_o| - |F_c||/\Sigma|F_o|$ and $wR_2 = [\Sigma w(Fo^2 - Fc^2)^2/ \Sigma wF_o^4]^{1/2}$.

Table S2. Crystal data and structure refinements for **$[Na_3(H_2O)_2][H_2N(CH_2COO)_2]_3 \cdot H_2O$**.

Empirical formula	**$[Na_3(H_2O)_2][H_2N(CH_2COO)_2]_3 \cdot H_2O$**
Formula weight	519.31
Temperature (K)	293(2)
Crystal color	Colorless
Crystal dimensions	$0.5 \times 0.5 \times 0.5$ mm^3
Wavelength (Å)	1.54184
Crystal system	Monoclinic
Space group	$P2_1/n$
a / Å	13.9720(5)
b / Å	9.9663(3)
c / Å	16.7140(6)
α / °	90
β / °	110.171(4)
γ / °	90
Volume / Å^3	2184.67(14)
Z	4
ρ_{calcd} / g·cm^{-3}	1.579
μ / mm^{-1}	1.757
F(000)	1080.0
Scan mode	ω scan
Data / restraints / parameters	4606/0/303
2-Theta range for data collection	3.570 to 79.058
Limiting indices	$-15 \le h \le 17$, $-12 \le k \le 11$, $-21 \le l \le 21$
Reflections collected	24448
Independent reflections	4606 [R_{int}=0.0497, R_{sigma}=0.0402]
Completeness	97.6%
Goodness-of-fit on F^2	1.070
R_1,wR_2 ($I > 2\sigma$) [a]	R_1 = 0.0601, wR_2 = 0.1857
R_1,wR_2 (all data)	R_1 = 0.0783, wR_2 = 0.1703
Largest diff. peak and hole/ e·Å^{-3}	1.02 and -0.47
CCDC number	2393546

[a] $R_1 = \Sigma||F_o| - |F_c||/\Sigma|F_o|$ and $wR_2 = [\Sigma w(Fo^2 - Fc^2)^2/ \Sigma wF_o^4]^{1/2}$.

Table S3. Atomic coordinates, equivalent isotropic displacement parameters (Å^2) and BVS for **K[$H_2N(CH_2COO)_2$]**.

Atom	*Wyck.*	*x*	*Y*	*z*	U_{eq}[a]	BVS[b]
K1	2a	-307.6(12)	5033.6(17)	-1369.3(8)	27.9(3)	1.14
O1	2a	9661(7)	2616(5)	6206(4)	35.2(9)	1.63
O2	2a	10563(8)	2544(5)	3757(5)	37.7(10)	1.66
O3	2a	2964(5)	7582(4)	-117(4)	27.5(7)	1.78
O4	2a	6933(6)	7264(5)	231(4)	31.5(8)	1.87
N1	2a	7015(5)	4969(	2713(3)	21.6(5)	
C1	2a	9268(7)	2963(6)	4758(5)	26.8(8)	
C2	2a	6931(7)	3984(6)	4206(4)	27.7(8)	
C3	2a	4751(6)	5908(7)	2100(4)	25.8(8)	
C4	2a	4946(6)	7007(5)	608(4)	21.3(7)	

[a]U_{eq} is defined as 1/3 of the trace of the orthogonalised U_{ij} tensor.

[b]Bond valence sums were calculated by the equation： $s = \exp[(R_0 - R_i)/b]$, where R_0 and b are the bond valence parameters and R_i is the observed bond lengths.

Table S4. Anisotropic displacement parameters (Å^2) for **K[$H_2N(CH_2COO)_2$]**..

Atom	U_{11}	U_{22}	U_{33}	U_{23}	U_{13}	U_{12}
K1	0.0304(4)	0.0257(4)	0.0287(4)	-0.0015(4)	0.0076(3)	-0.0023(4)
O1	0.0439(18)	0.039(2)	0.0208(18)	0.0046(13)	-0.0013(14)	0.0146(15)
O2	0.044(2)	0.040(3)	0.030(2)	0.0060(15)	0.0073(14)	0.0175(16)
O3	0.024(15)	0.0277(17)	0.0294(17)	0.0073(12)	0.0001(12)	0.0024(11)
O4	0.0271(16)	0.0334(17)	0.0354(18)	0.0083(14)	0.0097(13)	0.0016(13)
N1	0.0232(11)	0.0202(12)	0.0211(12)	0.0021(16)	0.0023(9)	0.0032(17)
C1	0.0336(19)	0.0199(18)	0.024(2)	-0.0010(16)	-0.0041(15)	0.0042(15)
C2	0.0268(18)	0.034(2)	0.0223(18)	0.0055(17)	0.0026(15)	0.0037(15)
C3	0.0241(16)	0.0298(19)	0.0239(18)	0.0068(16)	0.0051(14)	0.0057(15)
C4	0.0264(17)	0.0174(17)	0.0199(17)	-0.002 (15)	0.0034(14)	0.002(14)

Table S5. Selected bond lengths (**Å**) and angles (deg.) for **K[$H_2N(CH_2COO)_2$]**.

K(1)-O(1)$^{\#2}$	2.715(4)	K(1)-O(3)$^{\#1}$	2.755(3)
K(1)-O(2)$^{\#3}$	2.723(4)	K(1)-O(4)$^{\#4}$	2.750(4)
K(1)-O(3)	2.712(3)	K(1)-O(4)$^{\#5}$	2.831(4)
O(1)$^{\#2}$-K(1)-O(2)$^{\#3}$	81.38(8)	O(3)-K(1)-O(2)$^{\#3}$	78.92(10)
O(1)$^{\#2}$- K(1)-O(3)$^{\#1}$	90.40(11)	O(3)-K(1)-O(3)$^{\#1}$	129.49(5)
O(1)$^{\#2}$- K(1)-O(4)$^{\#4}$	145.13(10)	O(3)-K(1)-O(4)$^{\#4}$	79.20(10)
O(1)$^{\#2}$- K(1)-O(4)$^{\#5}$	75.05(10)	O(3)-K(1)-O(4)$^{\#5}$	87.27(7)
O(2)$^{\#3}$- K(1)-O(3)$^{\#1}$	143.53(10)	O(3)$^{\#2}$-K(1)-O(4)$^{\#5}$	77.08(9)
O(2)$^{\#3}$- K(1)-O(4)$^{\#4}$	91.28(12)	O(4)$^{\#5}$-K(1)-O(3)$^{\#1}$	75.46(8)

O(2)$^{\#3}$-K(1)-O(4)$^{\#5}$	133.16(12)	O(4)$^{\#5}$-K(1)-O(4)$^{\#5}$	129.91(5)
O(3)-K(1)-O(1)$^{\#2}$	131.57(12)		

Symmetry transformations used to generate equivalent atoms: #1 - x, - 1/2 + y, - z; #2 -1 + x, y, -1 + z; #3 1 - x, 1/2 + y, - z; #4 - 1 + x, y, z; #5 1 - x, - 1/2 + y, - z

Table S6. Atomic coordinates, equivalent isotropic displacement parameters (Å^2) and BVS for **[Na$_3$(H$_2$O)$_2$][H$_2$N(CH$_2$COO)$_2$]$_3$·H$_2$O**.

Atom	*Wyck.*	*x*	*y*	*z*	U_{eq}[a]	BVS[b]
Na1	4a	0.49681(6)	0.74943(8)	0.58032(5)	0.0254(2)	1.17
Na2	4a	0.48525(9)	1.04379(11)	0.70196(8)	0.0427(3)	1.00
Na3	4a	1.00492(6)	0.74273(8)	0.41882(5)	0.0263(2)	1.18
O1	4a	0.9149(14)	0.16323(18)	0.78125(11)	0.0358(4)	1.72
O2	4a	0.87313(7)	0.17037(5)	0.64005(5)	0.0315(8)	1.7
O3	4a	0.61812(12)	0.43748(16)	0.45835(10)	0.0290(4)	1.65
O4	4a	0.58576(14)	0.63908(16)	0.50151(11)	0.0348(4)	1.69
O5	4a	0.62685(12)	0.14734(16)	0.36228(10)	0.0296(4)	1.73
O6	4a	0.57863(14)	0.14425(17)	0.22088(11)	0.0336(4)	1.80
O7	4a	0.43591(17)	0.43591(17)	0.53679(11)	0.0312(4)	1.63
O8	4a	0.91171(15)	0.63121(17)	0.49173(12)	0.0372(4)	1.73
O9	4a	0.92687(14)	0.95788(17)	0.39186(12)	0.0349(4)	1.70
O10	4a	0.88455(13)	1.14442(16)	0.44626(11)	0.0312(4)	1.58
O11	4a	0.61141(13)	1.14382(16)	0.55095(11)	0.0305(4)	1.63
O12	4a	0.57646(14)	0.96552(17)	0.6171(12)	0.0341(4)	1.91
O13	4a	1.0105(2)	1.0764(2)	0.28828(18)	0.0602(6)	
O14	4a	0.4063(2)	1.2486(2)	0.65084(15)	0.0628(7)	
O15	4a	0.5833(3)	1.1516(3)	0.82617(17)	0.0838(9)	
N1	4a	0.73467(14)	0.36076(18)	0.61545(11)	0.0244(4)	
N2	4a	0.75418(14)	0.35527(18)	0.3819(11)	0.0248(4)	
N3	4a	0.75537(13)	1.01688(19)	0.50701(11)	0.0253(4)	
C1	4a	0.86541(17)	0.2096(2)	0.70942(13)	0.0247(4)	
C2	4a	0.7866(2)	0.3162(3)	0.70451(14)	0.0323(5)	
C3	4a	0.6718(2)	0.4834(2)	0.607(15)	0.0336(5)	
C4	4a	0.62123(16)	0.5232(2)	0.51397(14)	0.0237(4)	
C5	4a	0.62892(16)	0.1908(2)	0.29164(13)	0.0237(4)	
C6	4a	0.6982(2)	0.3096(3)	0.26349(14)	0.0337(5)	
C7	4a	0.8152(2)	0.4785(3)	0.38717(16)	0.0364(6)	
C8	4a	0.87084(17)	0.519(2)	0.48019(15)	0.0258(5)	
C9	4a	0.88161(16)	1.0203(2)	0.43258(14)	0.0242(4)	
C10	4a	0.8193(2)	0.9340(2)	0.47177(17)	0.0324(5)	
C11	4a	0.6964(2)	0.9373(2)	0.54898(18)	0.035(6)	
C12	4a	0.62145(16)	1.0237(2)	0.5745(14)	0.0236(4)	

[a]U_{eq} is defined as 1/3 of the trace of the orthogonalised U_{ij} tensor.

[b]Bond valence sums were calculated by the equation：$s = \exp[(R_0 - R_i)/b]$, where R_0 and b are the bond valence parameters and R_i is the observed bond lengths.

Table S7. Anisotropic displacement parameters (Å^2) for **$[Na_3(H_2O)_2][H_2N(CH_2COO)_2]_3 \cdot H_2O$**.

Atom	U_{11}	U_{22}	U_{33}	U_{23}	U_{13}	U_{12}
Na1	0.0278(5)	0.0232(5)	0.0252(5)	-0.0022(3)	0.0093(4)	0.000(3)
Na2	0.0446(6)	0.0385(6)	0.0469(6)	-0.0022(5)	0.0184(5)	-0.0027(4)
Na3	0.028 (5)	0.0241(5)	0.0273(5)	0.0018(3)	0.0102(4)	0.0002(3)
O1	0.0428(10)	0.0379(9)	0.0236(8)	0.0082(7)	0.0076(7)	0.0031(8)
O2	0.0311(8)	0.0387(9)	0.024(8)	-0.0033(7)	0.0088(7)	0.0018(7)
O3	0.0331(8)	0.0264(8)	0.0278(8)	-0.0059(6)	0.011 (7)	0.0003(6)
O4	0.0484(10)	0.0244(8)	0.0349(9)	0.0032(7)	0.0187(8)	0.0116(7)
O5	0.0309(8)	0.0335(9)	0.0241(8)	0.0019(6)	0.0092(6)	-0.0036(6)
O6	0.0404(9)	0.0343(9)	0.023(8)	-0.0065(7)	0.0067(7)	-0.003 (7)
O7	0.0329(8)	0.0318(9)	0.0287(8)	0.0075(7)	0.0105(7)	-0.0025(7)
O8	0.0488(10)	0.0254(8)	0.0401(10)	-0.0048(7)	0.019(8)	-0.013 (7)
O9	0.0444(10)	0.0291(8)	0.0402(10)	-0.0007(7)	0.0262(8)	0.0064(7)
O10	0.0332(9)	0.0204(8)	0.0412(10)	-0.0017(6)	0.0144(7)	0.0009(6)
O11	0.0334(9)	0.022(8)	0.0373(9)	0.0044(6)	0.0138(7)	0.0015(6)
O12	0.0404(10)	0.0294(9)	0.0407(10)	0.0013(7)	0.0243(8)	-0.0057(7)
O14	0.0869(18)	0.0472(13)	0.0487(13)	0.0053(10)	0.0162(12)	-0.0008(11)
O15	0.102(2)	0.082(2)	0.0535(15)	0.0066(14)	0.0083(15)	-0.0033(16)
N1	0.0306(9)	0.0225(9)	0.0202(8)	-0.001(7)	0.0088(7)	0.0031(7)
N2	0.0306(10)	0.0233(9)	0.0206(9)	0.0011(7)	0.0091(7)	-0.0029(7)
N3	0.0316(10)	0.0196(9)	0.0285(10)	-0.0004(7)	0.0152(8)	-0.001(7)
C1	0.0264(10)	0.0251(10)	0.0213(10)	0.0003(8)	0.0065(8)	-0.0048(8)
C2	0.042 (13)	0.0353(12)	0.0193(10)	0.0011(9)	0.0102(10)	0.0078(10)
C3	0.0451(13)	0.029(12)	0.0274(11)	-0.0032(9)	0.0132(10)	0.0111(10)
C4	0.0233(10)	0.0215(10)	0.028(11)	-0.0004(8)	0.0112(8)	-0.0004(8)
C5	0.0261(10)	0.0234(10)	0.0216(10)	-0.0001(8)	0.008 (8)	0.003 (8)
C6	0.0459(14)	0.0337(12)	0.0199(10)	-0.0002(9)	0.0092(10)	-0.0105(10)
C7	0.0496(15)	0.031(12)	0.0287(12)	0.0024(10)	0.0135(11)	-0.0156(11)
C8	0.026(10)	0.0254(10)	0.0287(11)	-0.0003(9)	0.0128(9)	-0.0006(8)
C9	0.023(10)	0.0232(10)	0.0254(10)	0.0015(8)	0.0072(8)	0.0027(8)
C10	0.0415(13)	0.0209(10)	0.043(13)	-0.0021(9)	0.025 (11)	0.0015(9)
C11	0.0452(14)	0.0221(11)	0.0492(15)	0.0038(10)	0.0309(12)	0.0009(10)
C12	0.0252(10)	0.0218(10)	0.0236(10)	-0.0029(8)	0.0081(8)	-0.0047(8)
O13	0.0746(16)	0.0524(13)	0.0682(16)	0.0066(12)	0.0431(13)	0.0111(12)

Table S8. Selected bond lengths (**Å**) and angles (deg.) for **$[Na_3(H_2O)_2][H_2N(CH_2COO)_2]_3 \cdot H_2O$**.

Na(1)-O(1)$^{\#1}$	2.3759(19)	Na(2)-O(14)	2.338(2)
Na(1)-O(3)$^{\#2}$	2.3979(18)	Na(2)-O(15)	2.319(3)
Na(1)-O(4)	2.3703(18)	Na(3)-O(2)$^{\#4}$	2.4037(19)
Na(1)-O(5)$^{\#2}$	2.4712(18)	Na(3)-O(6)$^{\#5}$	2.4286(19)
Na(1)-O(11)$^{\#3}$	2.4380(18)	Na(3)-O(7)$^{\#4}$	2.4154(19)
Na(1)-O(12)	2.4047(19)	Na(3)-O(8)	2.3475(19)
Na(2)-O(5) $^{\#2}$	2.4647(19)	Na(3)-O(9)	2.3773(18)
Na(2)-O(6) $^{\#2}$	2.601(2)	Na(3)-O(10)$^{\#6}$	2.5166(19)
Na(2)-O(12)	2.343(2)		
O(1)$^{\#1}$-Na(1)-O(3)$^{\#2}$	93.22(7)	O(15)-Na(2)-O(6)$^{\#2}$	95.03(9)
O(1)$^{\#1}$-Na(1)-O(5)$^{\#2}$	88.29(6)	O(15)-Na(2)-O(6)$^{\#2}$	95.03(9)
O(1)$^{\#1}$-Na(1)-O(11)$^{\#3}$	170.68(7)	O(15)-Na(2)-O(12)	110.87(9)
O(1)$^{\#1}$-Na(1)-O(12)	92.05(7)	O(15)-Na(2)-O(5)$^{\#2}$	146.97(10)
O(3)$^{\#2}$- Na(1)-O(5)$^{\#2}$	86.29(6)	O(15)-Na(2)-O(6)$^{\#2}$	95.03(9)
O(3)$^{\#2}$- Na(1)-O(11)$^{\#3}$	86.94(6)	O(15)-Na(2)-O(12)	114.97(10)
O(3)$^{\#2}$- Na(1)-O(12)	166.52(7)	O(15)-Na(2)-O(14)	88.93(11)
O(4)-Na(1)-O(1)$^{\#1}$	100.24(7)	O(2)$^{\#4}$-Na(3)-O(6)$^{\#5}$	85.73(6)
O(4)-Na(1)-O(3)$^{\#2}$	85.44(6)	O(2)$^{\#4}$-Na(3)-O(7)$^{\#4}$	81.77(6)
O(4)-Na(1)-O(5)$^{\#2}$	168.43(7)	O(2)$^{\#4}$-Na(3)-O(10)$^{\#6}$	84.45(6)
O(4)-Na(1)-O(11)$^{\#3}$	89.07(6)	O(6)$^{\#5}$-Na(3)-O(10)$^{\#6}$	170.10(7)
O(4)-Na(1)-O(12)	105.81(7)	O(7)$^{\#4}$-Na(3)-O(6)$^{\#5}$	93.07(6)
O(11)$^{\#3}$-Na(1)-O(5)$^{\#2}$	82.42(6)	O(7)$^{\#4}$-Na(3)-O(10)$^{\#6}$	84.30(6)
O(12)-Na(1)-O(5)$^{\#2}$	81.48(6)	O(8)-Na(3)-O(2)$^{\#4}$	168.98(8)
O(12)-Na(1)-O(11)$^{\#3}$	85.87(6)	O(8)-Na(3)-O(6)$^{\#5}$	97.99(7)
O(5)$^{\#2}$-Na(2)-O(6)$^{\#2}$	51.98(6)	O(8)-Na(3)-O(7)$^{\#4}$	87.65(7)
O(12)-Na(2)-O(5)$^{\#2}$	82.85(7)	O(8)-Na(3)-O(9)	103.01(7)
O(12)-Na(2)-O(6)$^{\#2}$	114.30(7)	O(8)-Na(3)-O(10)$^{\#6}$	97.45(6)
O(14)-Na(2)-O(5)$^{\#2}$	111.52(9)	O(9)-Na(3)-O(2)$^{\#4}$	86.61(6)
O(14)-Na(2)-O(6)$^{\#2}$	127.66(9)	O(9)-Na(3)-O(6)$^{\#5}$	98.35(7)
O(14)-Na(2)-O(12)	110.87(9)	O(9)-Na(3)-O(7)$^{\#4}$	163.06(7)
O(15)-Na(2)-O(5)$^{\#2}$	146.97(10)	O(9)-Na(3)-O(10)$^{\#6}$	82.32(6)

Symmetry transformations used to generate equivalent atoms: #1 3/2 - x, 1/2 + y, 3/2 - z; #2 1 - x, 1 - y,1 - z; #3 1 - x, 2 - y, 1 - z; #4 2 - x,1 - y, 1 - z; #5 3/2 - x, 1/2 + y, 1/2 - z; #6 2 - x, 2 - y, 1 - z; #7 3/2 - x, - 1/2 + y, 3/2 - z; #8 3/2 - x, - 1/2 + y, 1/2 - z

Table S9. The local dipole moment (μ) in Debye, as well as polarizability anisotropy ($\Delta\alpha$) for two **[$H_2N(CH_2COO)_2$]** groups in per unit cell of **K[$H_2N(CH_2COO)_2$]**. The charge of the structural group was estimated by the Bader charge of each atom.

Dipole moment	μ_x	μ_y	μ_z	μ	$\Delta\boldsymbol{\alpha}$
[$H_2N(CH_2COO)_2$]	-3.18	-0.20	2.41	4.00	5.30
[$H_2N(CH_2COO)_2$]	3.18	-0.20	-2.41	4.00	5.30
Total	0.00	-0.40	0.00		

Table S10. The first hyperpolarizability (β) in 10^{-30} esu for two **[$H_2N(CH_2COO)_2$]** groups in per unit cell of **K[$H_2N(CH_2COO)_2$]**.

β	**x**	**y**	**z**
[$H_2N(CH_2COO)_2$]	1.40	-0.15	-1.10
[$H_2N(CH_2COO)_2$]	-1.40	-0.15	1.10

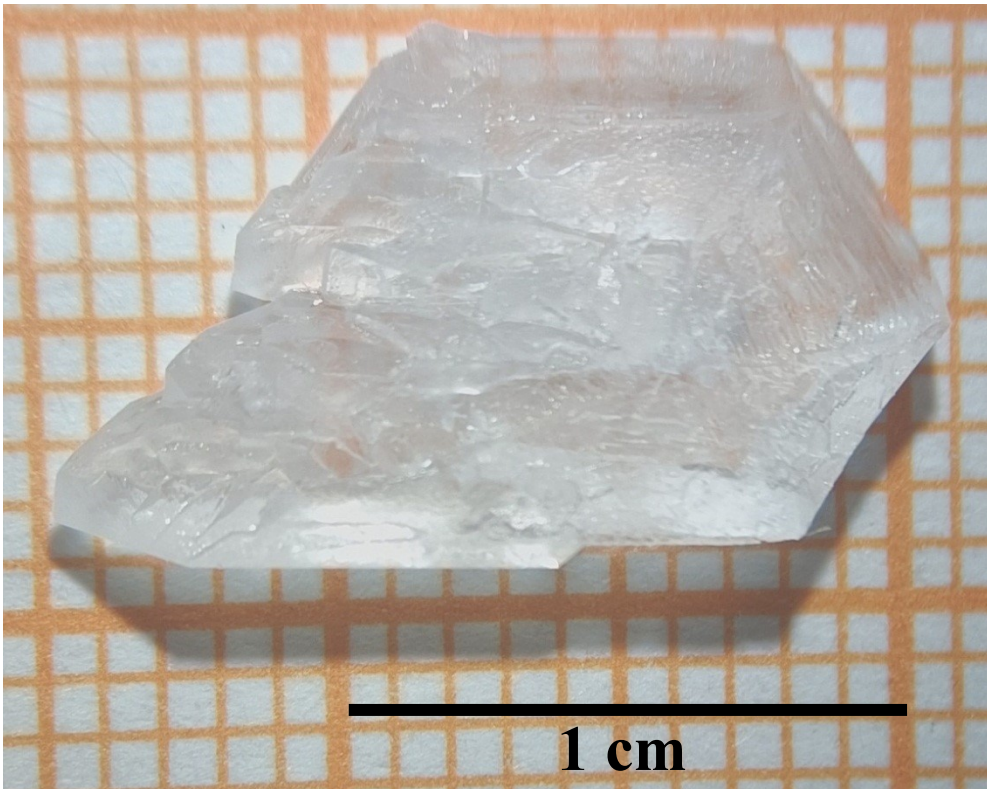

Figure S1. A photograph of the as-grown crystal without polishing for **$K[H_2N(CH_2COO)_2]$**.

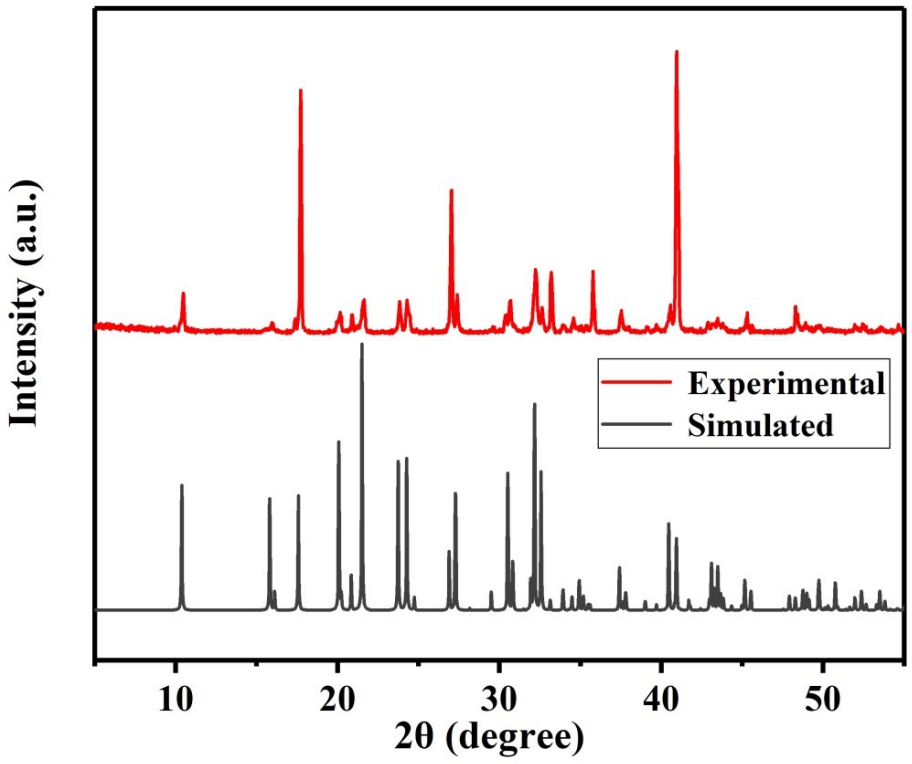

Figure S2. Experimental and simulated PXRD patterns of **K[$H_2N(CH_2COO)_2$]**.

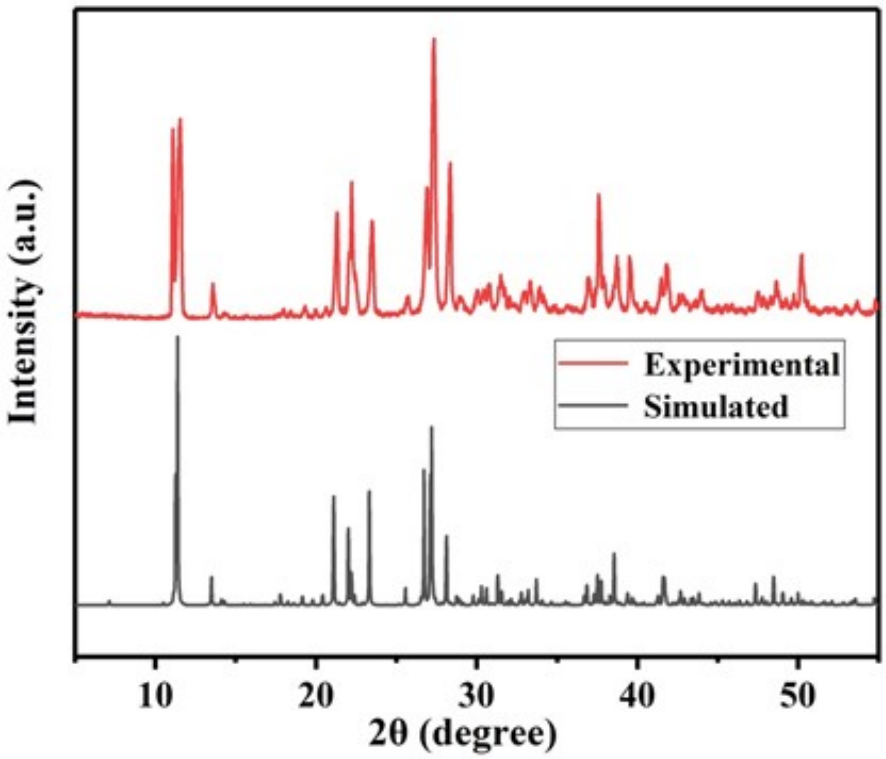

Figure S3. Experimental and simulated PXRD patterns of **[$Na_3(H_2O)_2$][$H_2N(CH_2COO)_2$]$_3$·H_2O**.

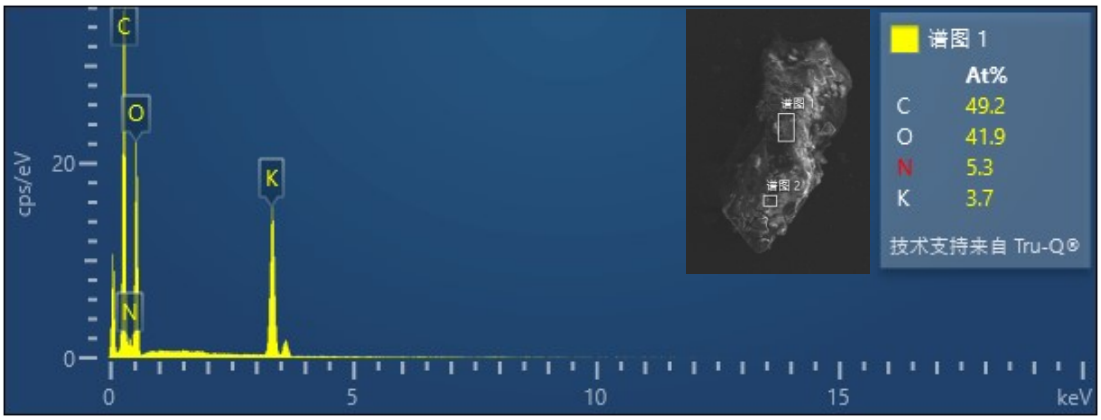

Figure S4. The EDS spectrum of **K[$H_2N(CH_2COO)_2$]**.

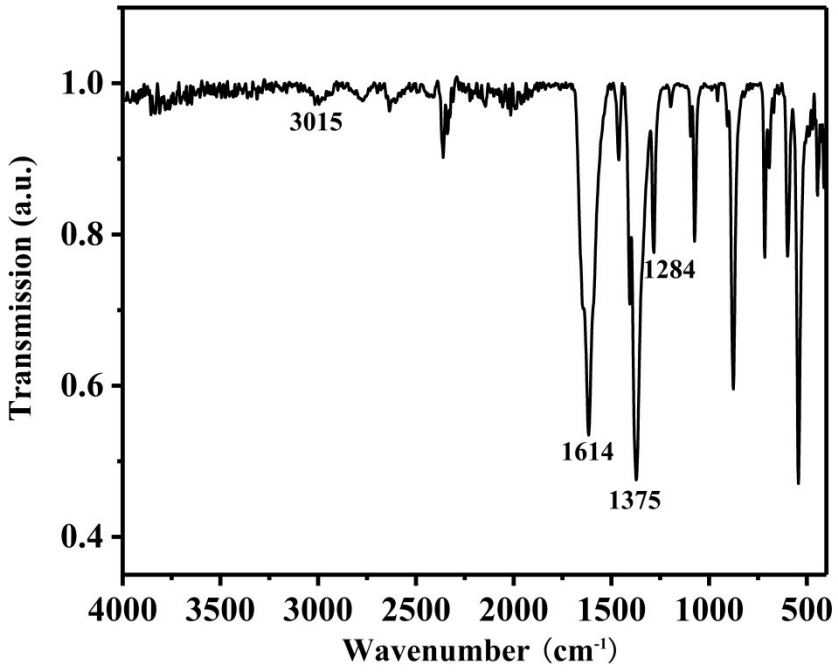

Figure S5. The IR spectrum of **K[$H_2N(CH_2COO)_2$]**.

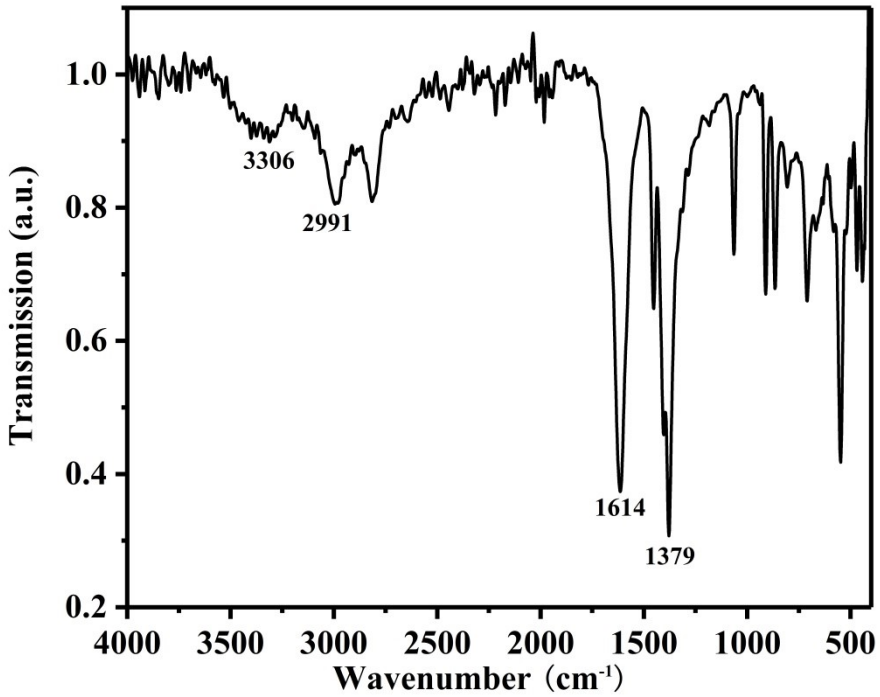

Figure S6. The IR spectrum of **[$Na_3(H_2O)_2$][$H_2N(CH_2COO)_2$]$_3$·H_2O**.

Figure S7. The $[NaO_n]$ (n = 5, 6) configurations. Symmetry codes: a 1/2 - x, 1/2 + y, 1/2 - z; b 1 - x, 1 - y, 1 - z; c 1 - x, 2 - y, 1 - z; d 2 - x, 1 - y, 1 - z; e 2 - x, 2 - y, 1 - z; f 3/2 - x, 1/2 + y, 1/2 - z.

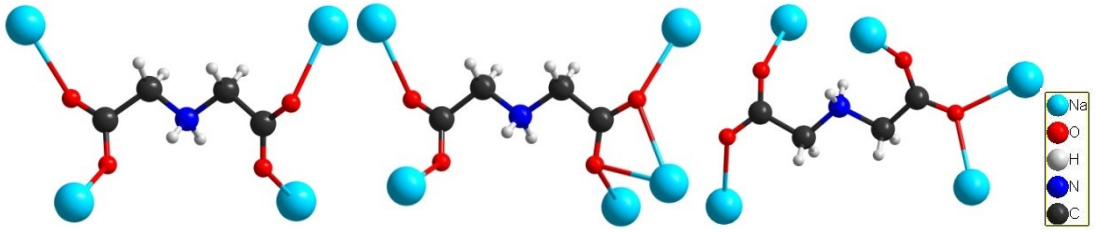

Figure S8. The environment of the $[H_2N(CH_2COO)_2]$ groups in **$[Na_3(H_2O)_2][H_2N(CH_2COO)_2]_3 \cdot H_2O$**.

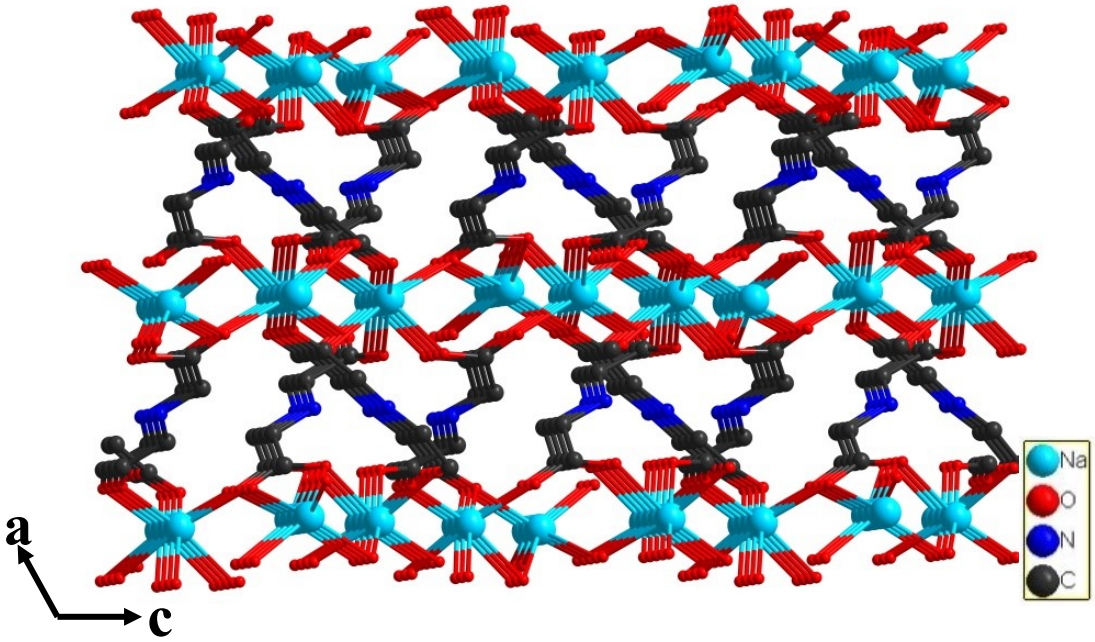

Figure S9. The 3D framework of **$[Na_3(H_2O)_2][H_2N(CH_2COO)_2]_3 \cdot H_2O$.**

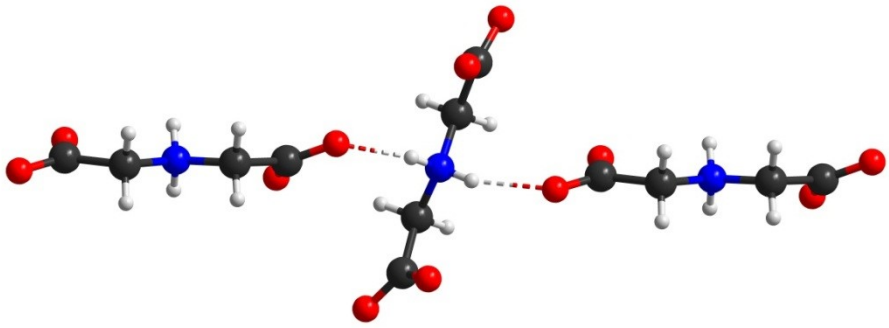

Figure S10. The hydrogen bondings among $[H_2N(CH_2COO)_2]$ groups in **$K[H_2N(CH_2COO)_2]$**. Symmetry codes: a 2 - x, 1/2 + y, 1 - z; b 1 - x, - 1/2 + y, - z.

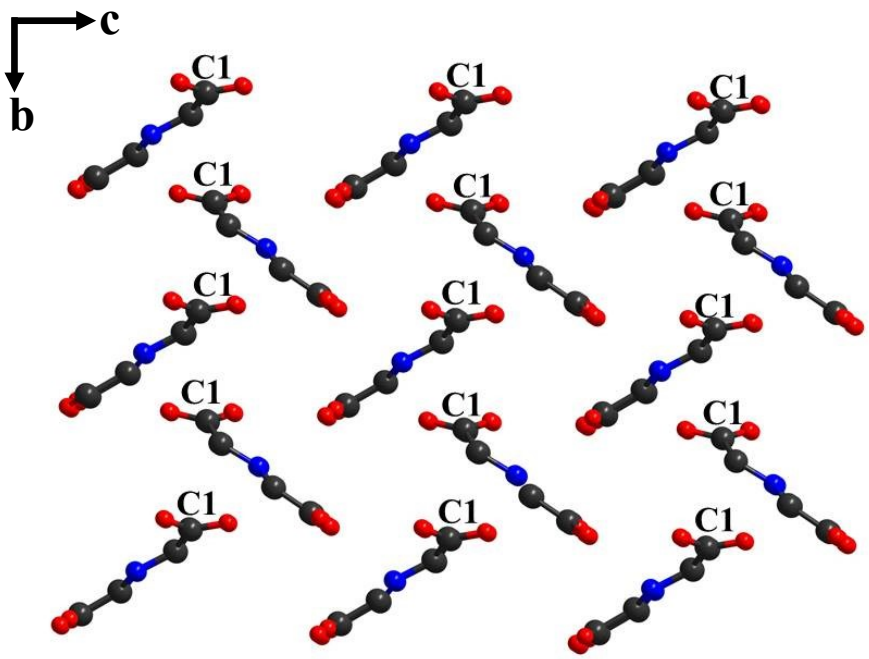

Figure S11. The ordered arrangement of $[H_2N(CH_2COO)_2]$ groups in **$K[H_2N(CH_2COO)_2]$**.

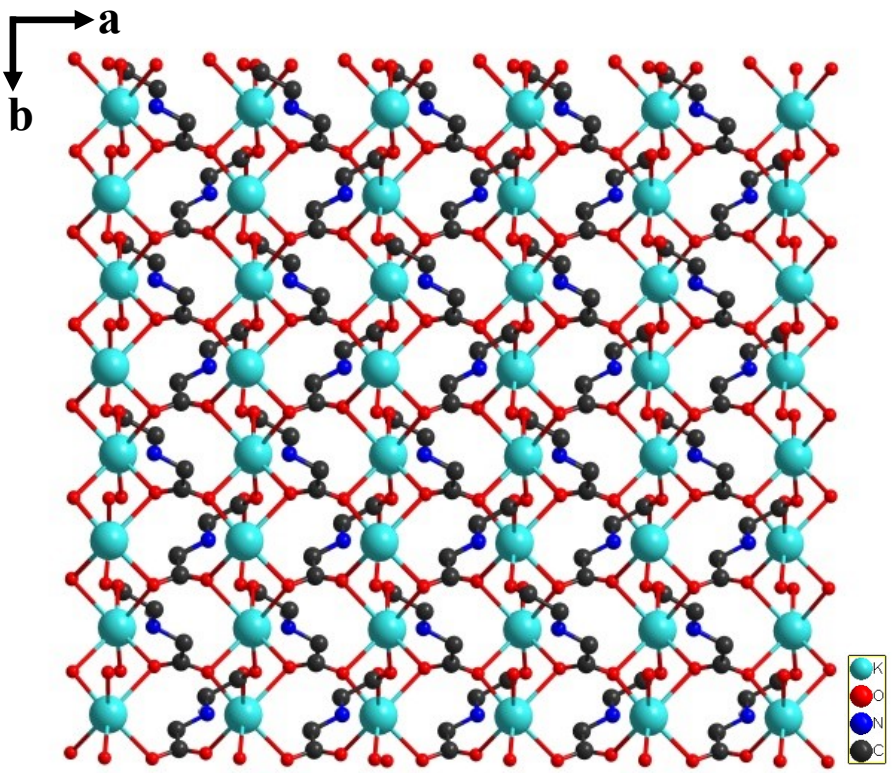

Figure S12. The 2D layer of **K[$H_2N(CH_2COO)_2$]**.

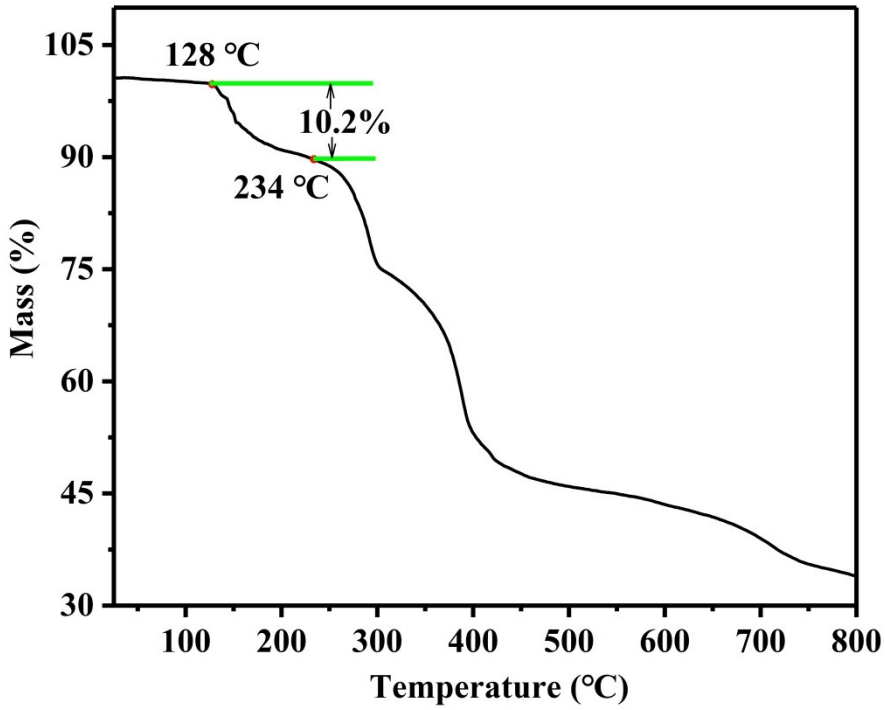

Figure S13. The TGA curve of **$[Na_3(H_2O)_2][H_2N(CH_2COO)_2]_3 \cdot H_2O$**.

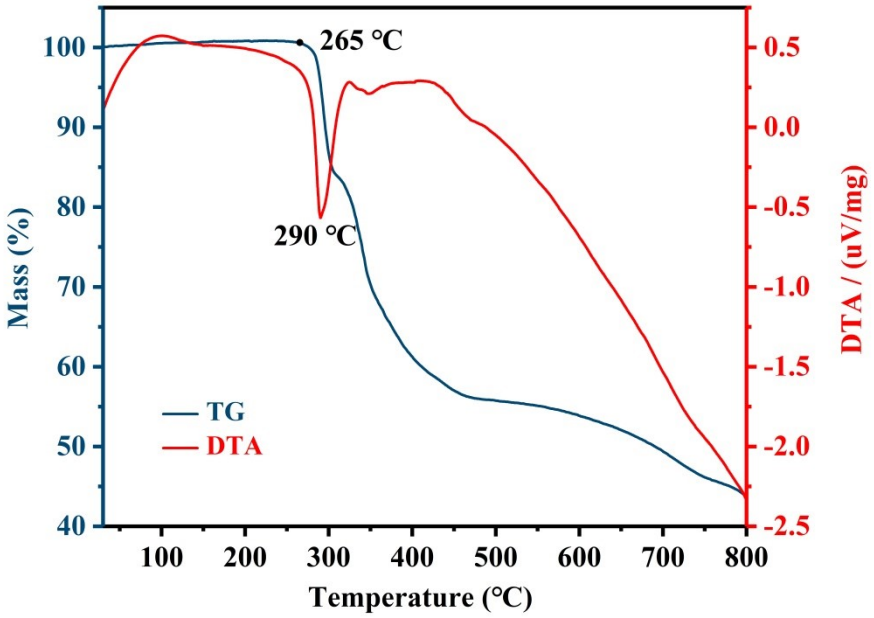

Figure S14. The TGA and DTA curves of **$K[H_2N(CH_2COO)_2]$**.

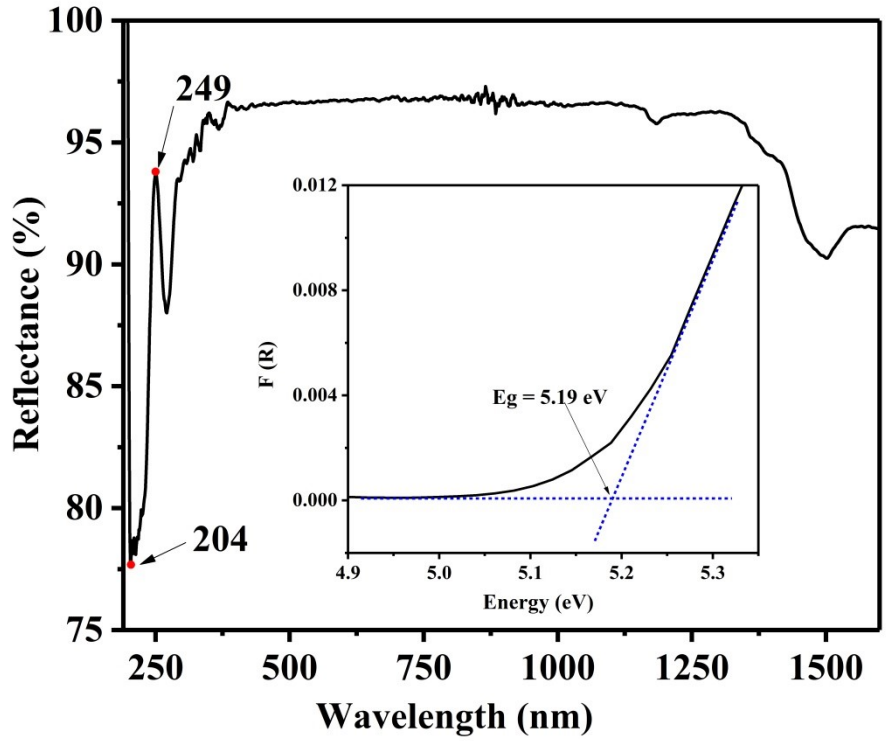

Figure S15. The UV-Vis–NIR spectrum of $[Na_3(H_2O)_2][H_2N(CH_2COO)_2]_3 \cdot H_2O$. Inset: the optical band gap.

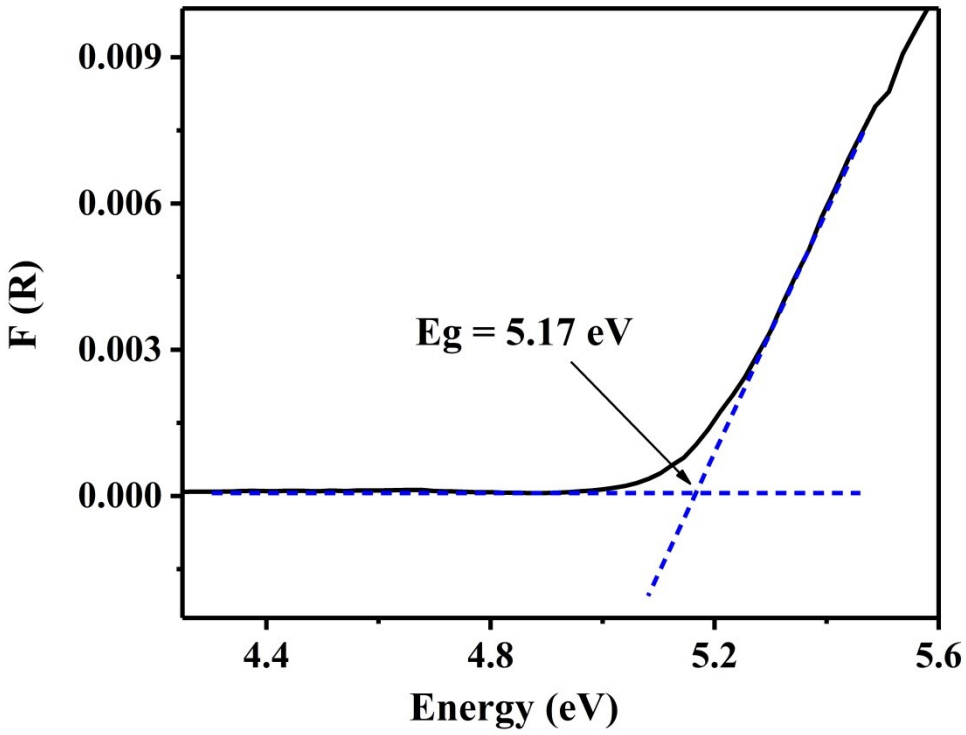

Figure S16. The optical band gap of $K[H_2N(CH_2COO)_2]$.

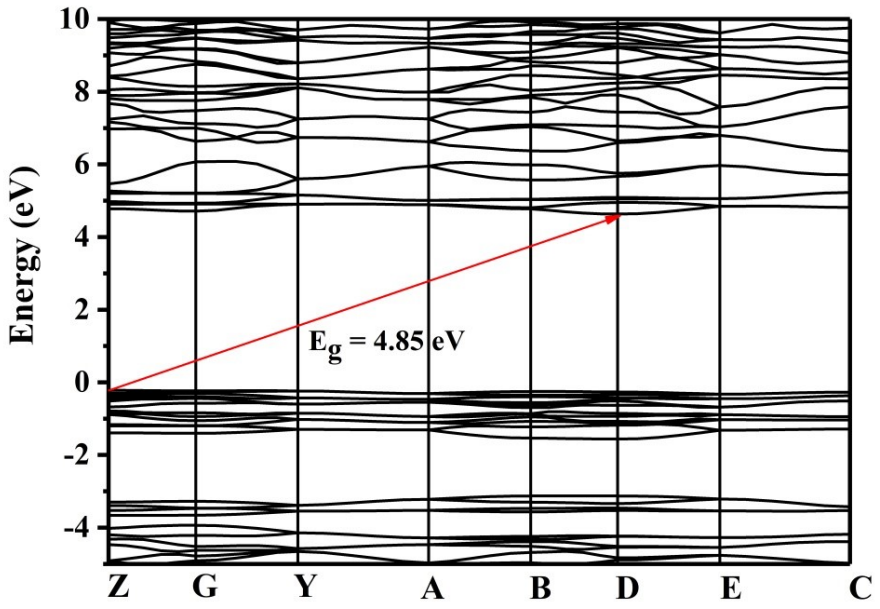

Figure S17. The calculated band structure of $K[H_2N(CH_2COO)_2]$.

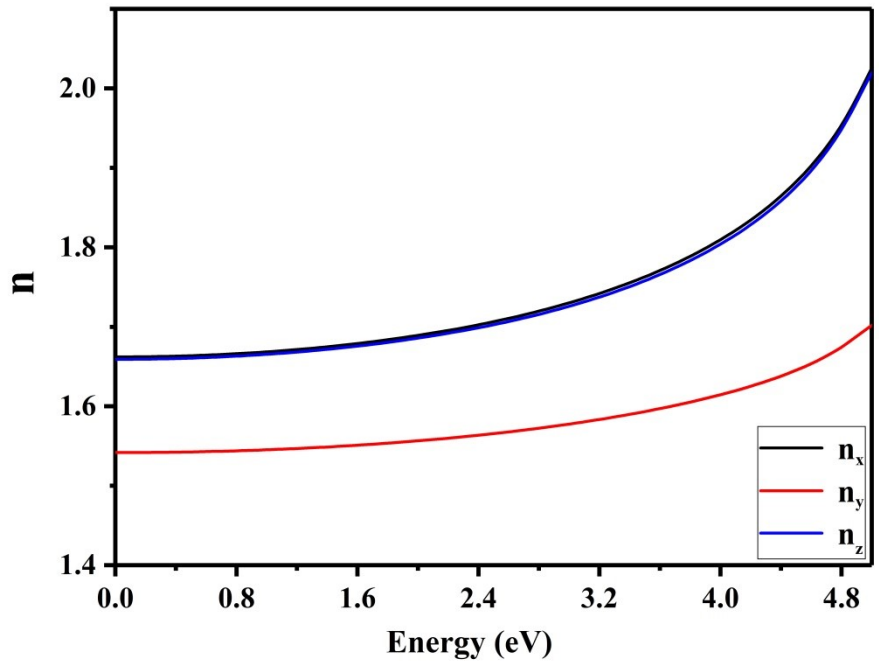

Figure S18. Optical refractive indices along principal axes *versus* photon energy for **$K[H_2N(CH_2COO)_2]$**.

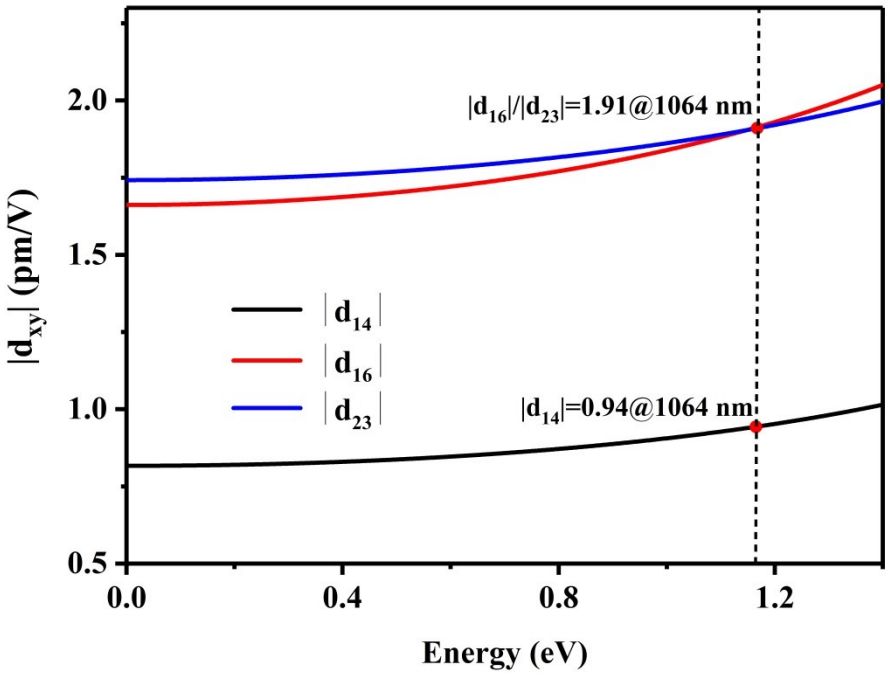

Figure S19. Frequency-dependent SHG coefficients of $|d_{14}|$, $|d_{16}|$ and $|d_{23}|$ for **$K[H_2N(CH_2COO)_2]$**.

References

1 G. M. Sheldrick, SHELXT-Integrated Space-Group and Crystal-Structure Determination, *Acta. Cryst.*, 2015, **A71**, 3-8.

2 G. M. Sheldrick, Crystal Structure Refinement with SHELXL, *Acta Cryst.*, 2015, **C71**, 3-8.

3 A. L. Spek, Single-Crystal Structure Validation with the Program PLATON, *J. Appl. Cryst.*, 2003, **36**, 7-13.

4 P. Kubelka, F. Munk, An Article on Optics of Paint Layers, *Z. Tech. Phys*., 1931, **12**, 259-274.

5 J. Tauc, Absorption Edge and Internal Electric Fields in Amorphous Semiconductors, *Mater. Res. Bull.*, 1970, **5**, 721-729.

6 S. Kurtz, T. Perry, A Powder Technique for the Evaluation of Nonlinear Optical Materials, *J. Appl. Phys.* 1968, **39**, 3798-3813.

7 G. Kresse, J. Furthmuller, Efficient Iterative Schemes for ab Initio Total-Energy Calculations using a Plane-Wave Basis set, *Phys. Rev. B.*, 1996, **54**, 11169-11186.

8 G. Kresse, D. Joubert, From Ultrasoft Pseudopotentials to the Projector Augmented-Wave Method, *Phys. Rev. B.*, 1999, **59**, 1758-1775.

9 J. P. Perdew, K. Burke, M, Generalized Gradient Approximation Made Simple, *Phys. Rev. Lett*., 1996, **77**, 3865-3868.

10 P. E. Blochl, Projector Augmented-Wave Method, *Phys. Rev. B.*, 1994, **50**, 17953-17979.

11 H. J. Monkhorst, J. D. Pack, Special Points for Brillouin-Zone Integrations, *Phys. Rev. B.*, 1976, **13**, 5188-5192.

12 C. Aversa, J. E. Sipe, Nonlinear Optical Susceptibilities of Semiconductors: Results with a Length-Gauge Analysis, *Phys. Rev. B.*, 1995, **52**, 14636-14645.

13 S. N. Rashkeev, W. R. L. Lambrecht, B. Segall, Efficient ab Initio Method for the Calculation of Frequency-Dependent Second-Order Optical Response in Semiconductors, *Phys. Rev. B.*, 1998, **57**, 3905-3919.

14 Z. Ma, J. Hu, R. Sa, Q. Li, Y. Zhang, K. Wu, Screening Novel Candidates for Mid-IR Nonlinear Optical Materials from I_3–V–VI_4 Compounds, *J. Mater. Chem. C*., 2017, **5**, 1963-1972.

15 Z. Fang, J. Lin, R. Liu, P. Liu, Y. Li, X. Huang, K. Ding, L. Ning, Y. Zhang, Computational Design of Inorganic Nonlinear Optical Crystals Based on a Genetic Algorithm, *Cryst. Eng. Comm*., 2014, **16**, 10569-10580.

16 Y. C. Yang, X. Liu, J. Lu, L. M. Wu, L. Chen, $[Ag(NH_3)_2]_2SO_4$: A Strategy for the Coordination of Cationic Moieties to Design Nonlinear Optical Materials, *Angew. Chem. Int. Ed.*, 2021, **60**, 21216-21220.

17 B. Champagne, D. M. Bishop, Calculations of Nonlinear Optical Properties for the Solid, *Adv. Chem. Phys*., 2003, **126**, 41-92.

18 A. H. Reshak, S. Auluck, I. V. Kityk, Specific Features in the Band Structure and Linear and Nonlinear Optical Susceptibilities of $La_2CaB_{10}O_{19}$ Crystals, *Phys. Rev. B*., 2007, **75**, 245120.

19 Y. Z. Huang, L. M. Wu, X. T. Wu, L. H. Li, L. Chen, Y. F. Zhang, $Pb_2B_5O_9I$: An Iodide Borate with Strong Second Harmonic Generation, *J. Am. Chem. Soc*., 2010, **132**, 12788-12789.

20 F. Weigend, R. Ahlrichs, Triple Zeta Valence and Quadruple Zeta Valence Quality for H to Rn: Design and assessment of accuracy, *Phys. Chem. Chem. Phys*., 2005, **7**, 3297-3305.

21 F. Weigend, Accurate Coulomb-Fitting Basis Sets for H to Rn, *Phys. Chem. Chem. Phys*., 2006, **8**, 1057-1065.

22 M. J. Frisch, G. W. Trucks, H. B. Schlegel, G. E. Scuseria, M. A. Robb, J. R. Cheeseman, G. Scalmani, V. Barone, G. A. Petersson, H. Nakatsuji, X. Li, M. Caricato, A. Marenich, J. Bloino, B. G. Janesko, R. Gomperts, B. Mennucci, H. P. Hratchian, J. V. Ortiz, A. F. Izmaylov, J. L. Sonnenberg, D. Williams-Young, F. Ding, F. Lipparini, F. Egidi, J. Goings, B. Peng, A. Petrone, T.

Henderson, D. Ranasinghe, V. G. Zakrzewski, J. Gao, N. Rega, G. Zheng, W. Liang, M. Hada, M. Ehara, K. Toyota, R. Fukuda, J. Hasegawa, M. Ishida, T. Nakajima, Y. Honda, O. Kitao, H. Nakai, T. Vreven, K. Throssell, J. A. Montgomery, Jr., J. E. Peralta, F. Ogliaro, M. Bearpark, J. J. Heyd, E. Brothers, K. N. Kudin, V. N. Staroverov, T. Keith, R. Kobayashi, J. Normand, K. Raghavachari, A. Rendell, J. C. Burant, S. S. Iyengar, J. Tomasi, M. Cossi, J. M. Millam, M. Klene, C. Adamo, R. Cammi, J. W. Ochterski, R. L. Martin, K. Morokuma, O. Farkas, J. B. Foresman, and D. J. Fox, Gaussian 09, Revision A.02, Gaussian, Inc., Wallingford CT, 2016.

23 T. Lu, F. Chen, A Multifunctional Wavefunction Analyzer, *J. Comput. Chem*., 2012, **33**, 580-592.